Shear wave speed structure beneath the South Pacific superswell using broadband data from ocean floor and islands

Takehi Isse,[1] Daisuke Suetsugu,[1] Hajime Shiobara,[2] Hiroko Sugioka,[1]
Kazunori Yoshizawa,[3] Toshihiko Kanazawa,[2] and Yoshio Fukao[1]

Received 11 May 2006; revised 28 June 2006; accepted 13 July 2006; published 17 August 2006.

[1] We determined three-dimensional shear wave speed structure beneath the South Pacific superswell down to a depth of 200 km by analyzing Rayleigh wave records from broadband ocean bottom seismograph stations and island stations in the Pacific Ocean. The ocean bottom stations were deployed from 2003 to 2005 on the seafloor in the French Polynesian region, which enabled us to study the upper mantle structure beneath the Superswell with unprecedentedly high resolution. We measured the dispersions of fundamental mode Rayleigh waves at periods between 40 and 140 seconds by the two-station method. We found pronounced slow anomalies near the hot spots and in the Lau Basin. The slow anomalies beneath the hot spots have deeper-rooted than those associated with the Lau basin. The slow anomalies near the Society, Macdonald, Marquesas, and Pitcairn hot spots continue down to at least 200 km depth. **Citation:** Isse, T., D. Suetsugu, H. Shiobara, H. Sugioka, K. Yoshizawa, T. Kanazawa, and Y. Fukao (2006), Shear wave speed structure beneath the South Pacific superswell using broadband data from ocean floor and islands, *Geophys. Res. Lett.*, *33*, L16303, doi:10.1029/2006GL026872.

1. Introduction

[2] The south Pacific superswell [*McNutt*, 1998] is characterized by a concentration of hotspot chains (e.g., Society, Cook-Austral, Marquesas and Pitcairn) and a large scale topographic high [e.g., *Adam and Bonneville*, 2005]. Previous seismic tomography studies show a broad low velocity anomaly in the lower mantle beneath the South Pacific, so-called Pacific superplume [*Larson*, 1991], which may indicate the presence of a large-scale upwelling, from the lower mantle to the surface. The relationship between the superplume and the south Pacific superswell is, however, still an open question, since the resolution of seismic tomography in the upper mantle of this region is poor due to a scarcity of seismic stations in the south Pacific.

[3] To improve the station coverage, we deployed a temporary array of long-term Broadband Ocean Bottom Seismographs (called BBOBSs hereafter) beneath the French Polynesian region from 2003 to 2005. In the present study we analyzed fundamental mode Rayleigh waves to determine 3-D shear wave speed structure in the upper mantle beneath the French Polynesian region with an unprecedented lateral resolution. The new 3-D model revealed low-speed anomalies associated with hot spots, some of which can be traced down to, at least, 200 km depth.

2. Data

[4] Since 1990s, BBOBSs have been developed and array observations by BBOBSs have been performed in the western Pacific as a part of the Ocean Hemisphere Project [*Kanazawa et al.*, 2001; *Shiobara et al.*, 2001]. *Isse et al.* [2004, 2006] analyzed Rayleigh waves using BBOBSs and land stations in the northwestern Pacific Ocean. This study has proved that the noise level of the vertical component BBOBS data is comparable to that of land stations.

[5] We deployed 8 BBOBSs in the period from 2003 to 2004 and 2 BBOBSs from 2004 to 2005 [*Suetsugu et al.*, 2005] (Figures 1a and 1b). Nine of the ten BBOBSs successfully recorded 10–12 months of data as planned. The BBOBS stations were equipped with the Guralp CMG-3T/EBB sensors which have a flat velocity response in period from 0.02 to 360 seconds and a 24 bit data acquisition system. The BBOBS can be operated for up to 400 days.

[6] In addition to the nine BBOBS stations, we used broadband or long period vertical-component seismograms at island stations around the study region including 10 IRIS stations, one GEOSCOPE station, 3 CEA stations (Commissariat à l'Energie Atomique) (Figures 1a and 1b). We analyzed events of body wave magnitudes greater than 5.5 occurring in and around the Pacific Ocean during the period from January, 1995 to May, 2005.

3. Method

[7] We employed the two-station method to measure dispersion of fundamental mode Rayleigh waves [*Dziewonski and Hales*, 1972]. When two stations are located nearly on a same great circle path from an earthquake, the phase speed dispersion between the stations can be determined by computing the phase differences of the surface wave pair. With this method we can ignore the effects of phase shift due to source excitation and lateral heterogeneity far outside the station-to-station path. We selected two-station pairs which meet the condition that the separation of the great circle paths to the stations is within the first Fresnel zone (Figures 1b and 1c). The average azimuthal difference between station-earthquake back-azimuth and the inter-station back-azimuth and

[1]Institute for Research on Earth Evolution, Independent Administrative Institution, Japan Agency for Marine-Earth Science and Technology, Yokosuka, Japan.
[2]Earthquake Research Institute, University of Tokyo, Tokyo, Japan.
[3]Department of Natural History Sciences, Hokkaido University, Sapporo, Japan.

0094-8276/06/2006GL026872

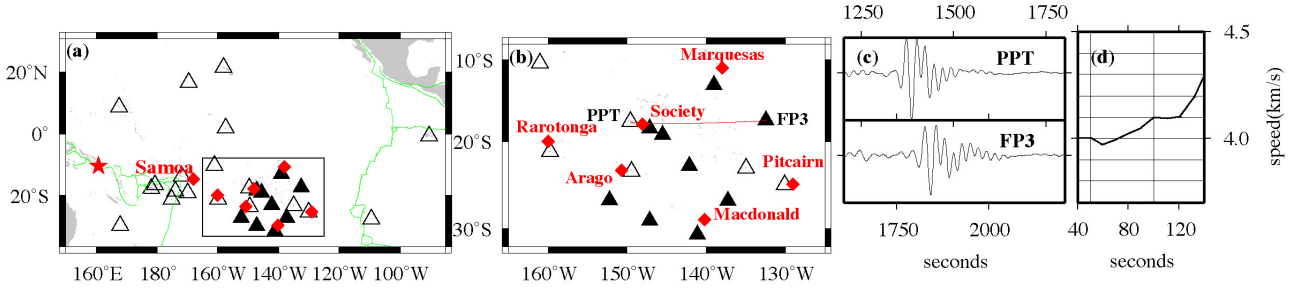

Figure 1. (a, b) Locations of stations and hotspots. Black triangles show the BBOBS stations, open triangles the island stations we used, red diamonds the hotspots in and around the Pacific superswell. (c) Example of paired Rayleigh wave records which are entered into the phase speed measurement by a two-station method. Event location is shown in Figure 1a by a star. The Rayleigh wave signal at BBOBS stations is comparable in quality to that at island stations. (d) Phase speed curve obtained along a ray path as in red in Figure 1b.

its standard deviation is $-0.2 \pm 3.5°$. We measured phase speed dispersion curves at periods from 40 to 140 seconds (Figure 1d), whose RMS errors [*Aki and Richards*, 2002] are less than 0.02 km/s. The number of obtained phase speed dispersion curves is 1317 at a period of 40 seconds and decreases with period down to 730 at 140 seconds. The number of phase speed dispersions obtained by BBOBS data is 10–15% of the total number.

[8] We inverted the measured phase speeds between station pairs for 2-D phase speed maps at periods from 40 to 140 seconds with a 10 seconds interval using the LSQR algorithm [*Paige and Saunders*, 1982]. The model space is parameterized using the B spline basis functions with an interval of 2.5°. We then inverted the dispersion curves for the shear wave speed model for each grid. We fixed the density and P wave speed structure to the reference model and solved only for shear wave speed, since the effects of density and P wave speed on Rayleigh wave phase speed perturbation are not significant [*Nataf et al.*, 1986]. The iterative least squares inversion by *Tarantola and Valette* [1982] is used for the inversion. We adopted parameters of a priori information on model amplitude and smoothness used by *Isse et al.* [2006] to suppress possible large perturbation and rough variation in the deeper part of the model where the fundamental mode data have poor resolution. The reference 1-D model is PREM [*Dziewonski and Anderson*, 1981] except for the crust for which we adopted the CRUST2.0 model [*Bassin et al.*, 2000].

4. Phase Speed Maps and Resolution Test

[9] Distributions of phase speed and its standard error at periods of 40 and 120 seconds are shown in Figures 2a and 2b. There are two pronounced slow speed anomalies at a period of 40 seconds: One is located in the Lau basin and the other is in the southern part of the superswell. The slow anomalies in the superswell persist at a period of 120 seconds, while those in the Lau basin weaken at the period. As the phase speed at longer periods reflect deeper part of the shear wave structures, the slow phase speed anomalies in the superswell appear to be deeper-rooted than those in the Lau basin. The standard errors of the phase speeds are less than 1% at periods of 40 and 120 seconds, respectively (Figures 2a and 2b). The amplitude of the obtained phase speed anomalies is much greater than the standard errors. Ray paths at a period of 90 seconds are shown in Figure 2c, demonstrating that the ray coverage in the French Polynesian region is improved by the BBOBS data.

[10] To see how phase speed maps could be resolved by the present path coverage, we performed ray-theoretical checkerboard resolution test with different cell sizes from 5° to 10°. Figures 3a–3d show the results of the checkerboard resolution test with 5° and 7.5° cells. The checkerboard pattern is well recovered especially in the region defined by the solid pentagon (Figures 3a and 3c). If the BBOBS stations were removed from this test, the resolvability is degraded significantly in the southern part of the

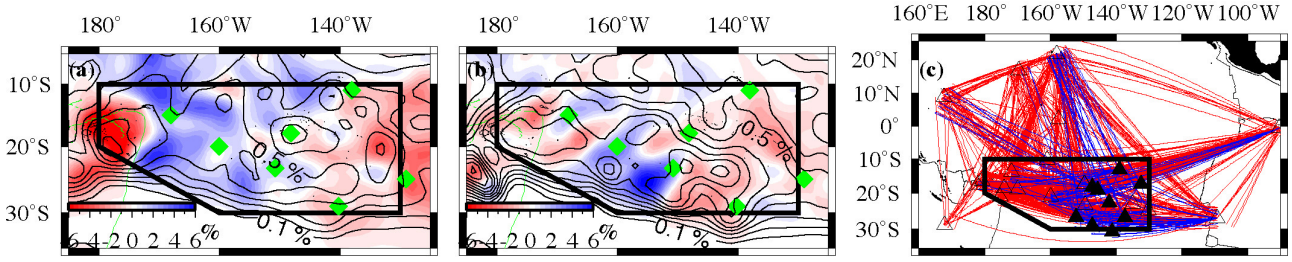

Figure 2. (a, b) Maps of phase speed anomalies and standard errors at periods of 40 and 120 seconds. The average phase speeds are 3.99 and 4.15 km/s, respectively. Green diamonds shows the hotspots. Color maps show phase speed and contours show the standard errors with 0.1% interval in each period. (c) Ray distributions we used. Solid and open triangles show the locations of BBOBS and island stations, respectively. Red lines show ray paths along which we measured the phase speeds using only island stations and blue lines using BBOBS stations.

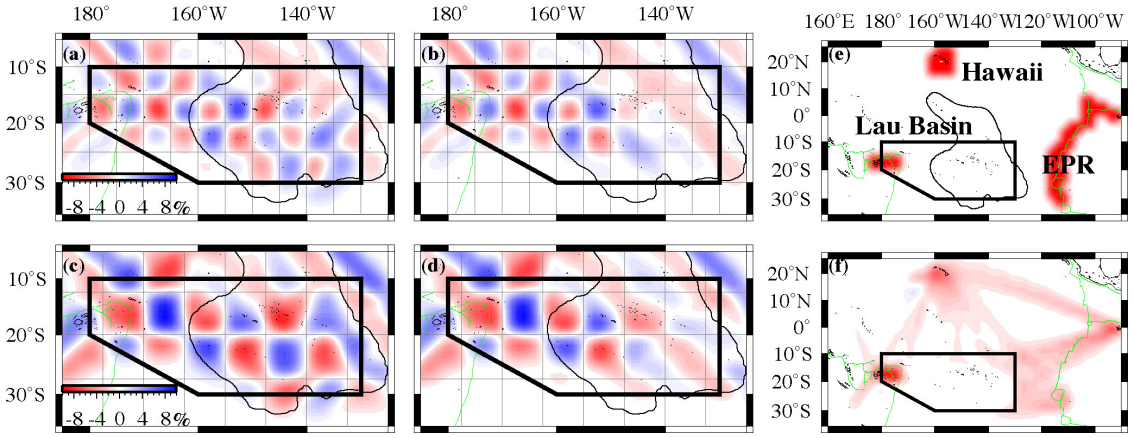

Figure 3. Checkerboard resolution test with (a, b) 5° and (c, d) 7.5° cell at a period of 40 seconds. Figures 3a and 3c show output models recovered by using all data and Figures 3b and 3d show those only by island data. Thin solid black line encircles the superswell region. Thick solid line shows the well-resolved region. The size of the input pattern are shown by grid and amplitude of the input patterns are ±10%. (e) Input slow phase speed anomalies beneath Hawaii, Lau basin and East Pacific Rise. (f) Output model.

superswell (Figures 3b and 3d). These are the features common to 10° cell size. Even though the number of BBOBS data is only 10–15% of the total data, the BBOBS data contribute substantially to improving our tomographic image of the superswell, because there are only four island stations in the superswell region in the present study. We roughly estimated the lateral resolution to be about 500 km beneath the southern part of the superswell from the above assessment.

[11] We also examined how the tomographic image in the superswell region could be distorted by artifacts due to speed anomalies outside the superswell. We constructed a hypothetical model in which we placed slow anomalies of −10% in the Hawaii islands, the Lau basin, and the East Pacific Rise, where the uppermost mantle is known to be anomalously slow [e.g., *Masters et al.*, 2000]. No anomalies were given anywhere else (Figure 3e). We tried to reconstruct the input hypothetical model using real ray paths to see how the known slow anomalies can be leaked into the image in the superswell. The output model (Figure 3f) shows that the artificial slow anomalies are as large as 1.5% in the easternmost part of the superswell and less than 1% in the southern part. Hereafter, we discuss the southern part of the Pacific superswell and its western extension, where checkerboard patterns are well recovered.

5. Results and Discussion

[12] Before going to details of the 3-D structure beneath the superswell, we computed the average shear wave speed profile beneath the superswell and compared to the PREM model and a previous model of the similar seafloor age in the Pacific Ocean (Figure 4a). The average profile was obtained by averaging 3-D shear speed structure in the superswell defined as the region of depth anomalies [*Adam and Bonneville*, 2005] greater than 300 m. The average speed profile beneath the entire Pacific Ocean with ages from 20 to 110 Ma was computed from the model by

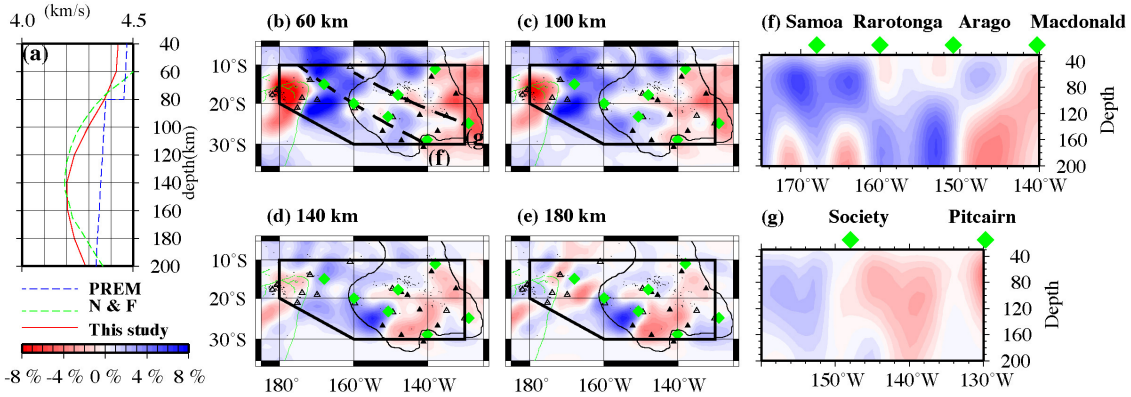

Figure 4. (a) Average shear speed profiles. Red solid line shows the average speed profile in the southern part of the Pacific superswell. Green broken line shows the profile by *Nishimura and Forsyth* [1989] for seafloor ages between 20 and 110 Ma in the whole Pacific (denoted by N&F). Blue is the isotropic PREM. Map projections of shear wave speed at depths (b) 60, (c) 100, (d) 140 and (e) 180 km. Thick solid line shows the well-resolved region. Thin solid line shows the region of the superswell defined by depth anomalies more than 300m. Tomographic cross-sections (f) along the Cook-Austral to Samoa hotspot trail and (g) along the Society to Pitcairn trail. Green diamonds show the locations of hotspots.

Nishimura and Forsyth [1989] for comparison. This age range is comparable to that of the superswell region (24–112 Ma). Figure 4a shows that the average shear wave speed beneath the Pacific superswell is significantly lower than PREM and similar to the average shear wave speed model beneath the entire Pacific. The similarity of the profile beneath the superswell to Nishimura and Forsyth's model is partially because their model for the seafloor ages of 20–110 Ma includes the superswell region.

[13] Figures 4b–4e are the shear wave speed maps at various depths down to 180 km. The reference structure is the average structure beneath the superswell (Figure 4a). Slowest anomalies of $-5 \sim -10\%$ are present in the Lau basin and to the east of the superswell at depths of 60 and 100 km. The former is associated with the back arc spreading in the Lau basin and the latter is partially attributed to relatively young ages of the seafloor. We can identify slow speed anomalies in the vicinity of most of the hot spots in the superswell region at depths shallower than 100 km (Figures 4b and 4c): slow anomalies of about -2% near the Society, Macdonald, Pitcairn, and Marquesas hot spots and about -1% near the Arago and Rarotonga hot spots. At depths greater than 100 km, slow anomalies beneath the Lau basin and to the east of the superswell tend to diminish. Most of the slow anomalies near the hot spots, on the other hand, can be traced down to at least 180 km depth (Figures 4d and 4e) and become even stronger ($-4 \sim -5\%$) than at shallower depths, particularly around the Macdonald Island chain. On the other hand, a shallow origin is suggested for the Arago and Rarotonga hot spots, where slow anomalies are identified only above 80 km depth. No anomalies are found immediately beneath Samoa. There are slow anomalies apparently not directly associated with any hot spots. One is at 25°S and 140°W between the Society and Pitcairn hot spots, and another at 20°S and 133°W between the Pitcairn and Marquesas hot spots. They can be seen at least down to 150 km depth.

[14] Figures 4f and 4g show the cross sections along the hot spot chains: one along the Cook-Austral chains and Samoa (Figure 4f), the other along the Society and Pitcairn chains (Figure 4g). Figure 4f shows different source depths for different hot spots. Beneath the Macdonald hot spot, slow anomalies are dipping to the west to extend down to 200 km depth, suggesting that a hot plume is uprising in an oblique manner. There are faint and shallow slow anomalies beneath Rarotonga and Arago. No slow anomalies are found immediately under the Samoa hot spot, where there are distinct slow anomalies at depths greater than 150 km. Along the Pitcairn-Society profile (Figure 4g), there is a sharp contrast across the Society hot spot, which separates fast anomalies to the west and slow anomalies to the east. The Pitcairn hot spot associates slow anomalies immediately underneath, while the slow anomalies under the Society hot spot have more complicated geometry. The slow anomaly near the Society hot spot at depths of 40–80 km at ~145°W appears to be linked to another slow anomaly at depths of 100–200 km located at ~140°W.

[15] Recent studies on the depths of the 410-km and 660-km discontinuities have suggested that hot anomalies are not widespread in the mantle transition zone (defined as the layer between the two discontinuities) beneath the superswell region, but are localized to the east of the Society hot spot [*Niu et al.*, 2002; *Suetsugu et al.*, 2004]. There is little evidence for such hot anomalies in the mantle transition zone beneath the other hot spots in the Superswell. On the other hand, the present study reveals slow speed anomalies (presumably hot anomalies) corresponding to all the hot spots in the superswell. It remains to be answered whether the hot anomaly in the mantle transition zone is linked or unlinked to the slow anomalies found in the upper 200 km of the mantle. A joint analysis of the BBOBS and land-based data including a temporary network like the PLUME network [*Barruol et al.*, 2002] should improve both depth and lateral resolution.

[16] **Acknowledgments.** We thank staffs of the IRIS, GEOSCOPE, CEA, and SPANET data center for their effort to maintain and manage the seismic stations. We also thank two anonymous reviewers for their helpful comments. This work was supported by Grant-in-Aid for Scientific Research (KAKENNHI, 16253002) from Japan Society for the Promotion Science. The GMT software package [*Wessel and Smith*, 1991] and SAC2000 [*Goldstein and Minner*, 1996] were used in this study.

References

Adam, C., and A. Bonneville (2005), Extent of the South Pacific Superswell, *J. Geophys. Res.*, *110*, B09408, doi:10.1029/2004JB003465.

Aki, K., and P. G. Richards (2002), *Quantitative Seismology*, 2nd ed., 700 pp., Univ. Sci., Sausalito, Calif.

Barruol, G., et al. (2002), PLUME investigates south pacific superswell, *Eos. Trans. AGU*, *83*(45), 511, 514.

Bassin, C., G. Laske, and G. Masters (2000), The current limits of resolution for surface wave tomography in North America, *Eos. Trans. AGU*, *81*(48), Fall Meet. Suppl., Abstract S12A-03.

Dziewonski, A. M., and D. L. Anderson (1981), Preliminary reference Earth model, *Phys. Earth Planet. Inter.*, *25*, 297–356.

Dziewonski, A. M., and A. L. Hales (1972), Numerical analysis of dispersed seismic waves, in *Seismology: Surface Waves and Earth Oscillations*, *Methods Comput. Phys.*, vol. 11, edited by B. A. Bolt, pp. 39–85, Elsevier, New York.

Goldstein, P., and L. Minner (1996), SAC2000: Seismic signal processing and analysis tools for the 21st century, *Seismol. Res. Lett.*, *67*, 39.

Isse, T., H. Shiobara, Y. Fukao, K. Mochizuki, T. Kanazawa, H. Sugioka, S. Kodaira, R. Hino, and D. Suetsugu (2004), Rayleigh wave phase velocity measurements across the Philippine Sea from a broadband OBS array, *Geophys. J. Int.*, *158*, 257–266, doi:10.1111/j.1365-246X.2004.02322.x.

Isse, T., et al. (2006), Three-dimensional shear wave structure beneath the Philippine Sea from land and ocean bottom broadband seismograms, *J. Geophys. Res.*, *111*, B06310, doi:10.1029/2005JB003750.

Kanazawa, T., H. Shiobara, M. Mochizuki, M. Shonohara, and E. Araki (2001), Seismic observation system on the sea floor, in *Proceedings of OHP/ION Joint Symposium, Long-Term Observations in the Oceans*, edited by B. Romanowicz, K. Suyehiro, and H. Kawakatsu, abstract S11-06, Earthquake Res. Inst., Univ. of Tokyo, Tokyo.

Larson, R. L. (1991), Latest pulse of Earth: Evidence for a mid-Cretaceous superplume, *Geology*, *19*, 547–550.

Masters, G., G. Laske, H. Bolton, and A. M. Dziewonski (2000), The relative behavior of shear velocity, bulk sound speed, and compressional velocity in the mantle: Implications for chemical and thermal structure, in *Earth's Deep Interior: Mineral Physics and Tomography From the Atomic to the Global Scale*, *Geophys. Monogr. Ser.*, vol. 117, edited by S. Karato et al., pp. 63–87, AGU, Washington D. C.

McNutt, M. (1998), Superswells, *Rev. Geophys.*, *36*, 211–244.

Nataf, H. C., I. Nakanishi, and D. L. Anderson (1986), Measurements of mantle wave velocities and inversion for lateral heterogeneities and anisotropy: 3. Inversion, *J. Geophys. Res.*, *91*(B7), 7261–7307.

Nishimura, C. E., and D. W. Forsyth (1989), The anisotropic structure of the upper mantle in the Pacific, *Geophys. J.*, *96*, 203–229.

Niu, F., S. C. Solomon, P. G. Silver, D. Suetsugu, and H. Inoue (2002), Mantle transition-zone structure beneath the South Pacific superswell and evidence for a mantle plume underlying the Society hotspot, *Earth Planet. Sci. Lett.*, *198*, 371–380.

Paige, C. C., and M. A. Saunders (1982), LSQR: An algorithm for sparse linear equations and sparse least squares, *Trans. Math. Software*, *8*, 43–71.

Shiobara, H., M. Kato, H. Sugioka, S. Yoneshima, K. Mochizuki, M. Mochizuki, S. Kodaira, R. Hino, M. Shinohara, and T. Kanazawa (2001), Long term observation by ocean bottom seismometer array on trans-PHS profile, in *Proceedings of OHP/ION Joint Symposium, Long-*

Term Observations in the Oceans, edited by B. Romanowicz, K. Suyehiro, and H. Kawakatsu, abstract S11-10, Earthquake Res. Inst., Univ. of Tokyo, Tokyo.

Suetsugu, D., T. Saita, H. Takenaka, and F. Niu (2004), Thickness of the mantle transition zone beneath the South Pacific as inferred from analyses of *ScS* reverberated and *Ps* converted waves, model, *Phys. Earth Planet. Inter.*, *146*, 35–46.

Suetsugu, D., et al. (2005), Probing South Pacific mantle plumes with broadband OBS, *Eos Trans. AGU*, *86*(44), 429, 435.

Tarantola, A., and B. Valette (1982), Generalized nonlinear inverse problems solved using the least-squares criterion, *Rev. Geophys.*, *20*, 219–232.

Wessel, P., and W. H. F. Smith (1991), Free software helps map and display data, *Eos. Trans. AGU*, *72*, 441, 445–446.

Y. Fukao, T. Isse, D. Suetsugu, and H. Sugioka, Institute for Research on Earth Evolution, Independent Administrative Institution, JAMSTEC, 2-15, Natsushima-cho, Yokosuka, Kanagawa 237-0061, Japan. (isse@jamstec.go.jp)

T. Kanazawa and H. Shiobara, Earthquake Research Institute, University of Tokyo, Yayoi 1-1-1, Tokyo Bunkyo-ku 113-0032, Japan.

K. Yoshizawa, Department of Natural History Sciences, Hokkaido University, Sapporo, 060-0810, Japan.